Norway grants

Ammonia as carbon free fuel for internal CombusTion engIne driVen AgriculTural vEhicle

ACTIVATE

Work Package 5
Deliverable Report

Topic: D5.8

Measurement data ready for publication from SI tests.

Programme operated by: NCBR National Centre for Research and Development

Project consortium: Silesian University of Technology; NTNU Norwegian University of Science and Technology; LOGE; University of Agriculture in Krakow

Norway grants

Contents

1 Pure ammonia fueled SI engine

This deliverable report presents experimental results and CFD model of premixed ammonia/air combustion in internal combustion engines, focusing on performance and exhaust pollutants. The test was carried out on a single-cylinder with spark-assisted compression ignition, which allows for a higher compression ratio of 16.5.

2 Introduction

Recent studies have found that ammonia can be used in spark-ignition (SI) engines. Lhuillier et al. [1] reported that a stable SI engine operation can be achieved for a stoichiometric NH3/air mixture. However, a small quantity of hydrogen is essential to guarantee stable engine operation in the wide ranges. They found that only mixtures with a high hydrogen fraction demonstrate suitability for extremely lean operation. With an increase in the NH_3 content of the fuel, the ignition timing must be advanced accordingly. As can be seen in figure 1, adjusting the timing of the spark becomes crucial to maintain cyclic stability and achieve maximum work output with the lowest ammonia emissions. Therefore, Figure 1 shows that pure ammonia operation can be achieved only when the ignition timing was set at -40 CAD. However, NH_3 emission is significantly high for pure ammonia around 10,000 ppm. However, adding a small amount of hydrogen can enhance the performance and stability of lean and rich mixtures and reduce unburned ammonia.

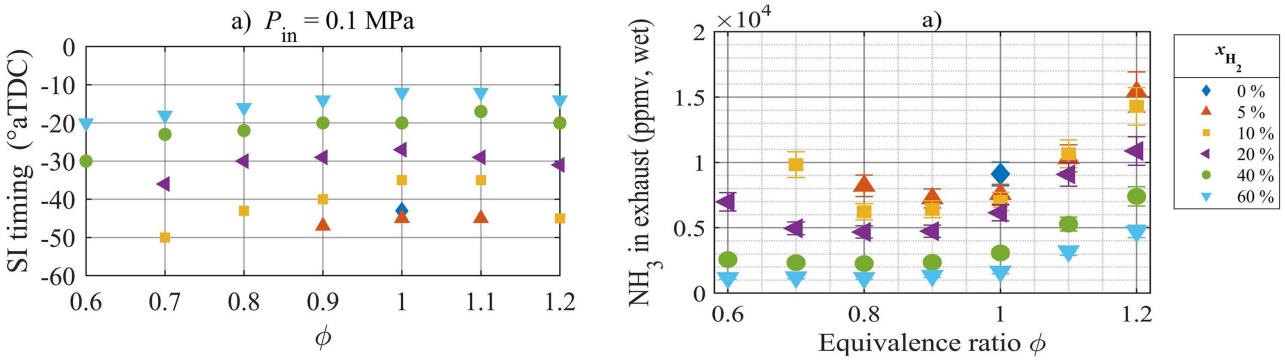

Figure 1: Optimized spark ignition timing for pure ammonia and added hydrogen for various ϕ as well as ammonia emission from Lhuillier et al. [1] paper.

Li et al. [2] experimentally studied the effects of ammonia and hydrogen mixture on combustion stabilities in SI optical engines. They illustrate representative flame images corresponding to different hydrogen-ammonia energy ratios in figure 2. The pure ammonia flame becomes visible around -8 CAD, due to the auto-ignition phenomenon. The ignition delay time for pure ammonia is significantly longer, leading to late combustion with low heat release. As a result, it becomes difficult to observe substantial early flame propagation, and the flame begins at approximately -8 CAD. They also mention that as the hydrogen-ammonia energy ratio increases, there is a noticeable advancement in the appearance of the initial flame kernel, indicating fast and early flame development. Furthermore,

the flame area at -8 CAD expands more rapidly as the hydrogen-ammonia energy ratio increases, suggesting faster flame propagation.

The HRR curves for different hydrogen-ammonia energy ratios were plotted by Li et al. [2]. They revealed a direct correlation: higher hydrogen-ammonia energy ratios correspond to increased peak heat release rates. The addition of hydrogen accelerates ammonia flame propagation, concentrating heat release and enhancing engine performance. The initial heat release phase shows that pure ammonia experiences a prolonged ignition delay time, while the mixture of ammonia and hydrogen shows a significantly shorter ignition delay time. Furthermore, it has been observed that increasing the hydrogen-ammonia energy ratio can significantly enhance the initial flame speed. However, adding 10% hydrogen can help overcome challenges related to ammonia combustion.

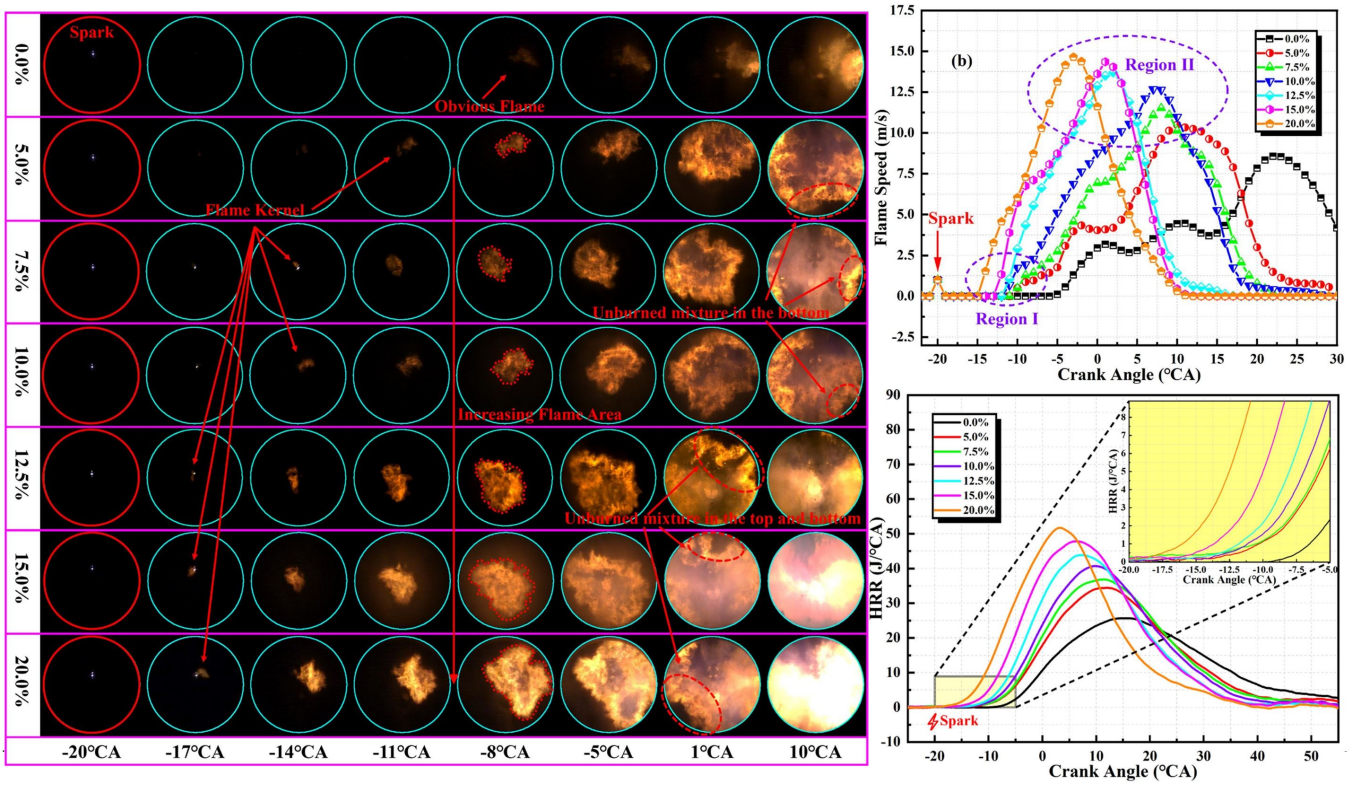

Figure 2: Images of flames of various hydrogen-ammonia energy ratios, flame speed and HRR from Li et al. [2]

3 CFD simulation Setup

The geometry and many of the case configurations for the CFD model have previously been published in our paper on ammonia biodiesel CI engine [3]. In addition, the mesh, the turbulence model and the boundary conditions are defined in the same way as described in our previous CFD paper [3]. The CFD model was implemented using the commercial code CONVERGE version 3.0 and Tecplot 360 for visualization.

The engine operating conditions for CFD simulation are defined as follows:

- Engine speed: 1500 rpm
- Ignition timing: -40 CAD
- Ammonia stoichiometric air mixture condition: $\phi = 1$
- AES: 100%
- Intake air temperature: 300 K, 350 K, and 400 K
- ignition energy : 0.05 J for 0.5 CAD duration
- Intake pressure: 1 bar
- Three different ammonia/ air combustion reaction mechanisms: a) Stagni et al. [4] b) GRI 3.0 [5] c) San Diego [6]

3.1 CFD results of pure ammonia fueled SI engine

Figure 3 illustrates the in-cylinder pressure, HRR, and mean temperature of the ammonia-fueled spark-ignition engine using three different reaction mechanisms: Stagni et al. [4], GRI 3.0 [5], and San Diego [6], as well as hot motoring operation. It is evident that the choice of reaction mechanism significantly affects the CFD results. The San Diego reaction mechanism tends to overestimate the cylinder pressure, complete combustion, and HRR peak. On the other hand, the Stagni and GRI 3.0 reactions for pure ammonia exhibit similar in-cylinder pressure and heat release rate patterns.

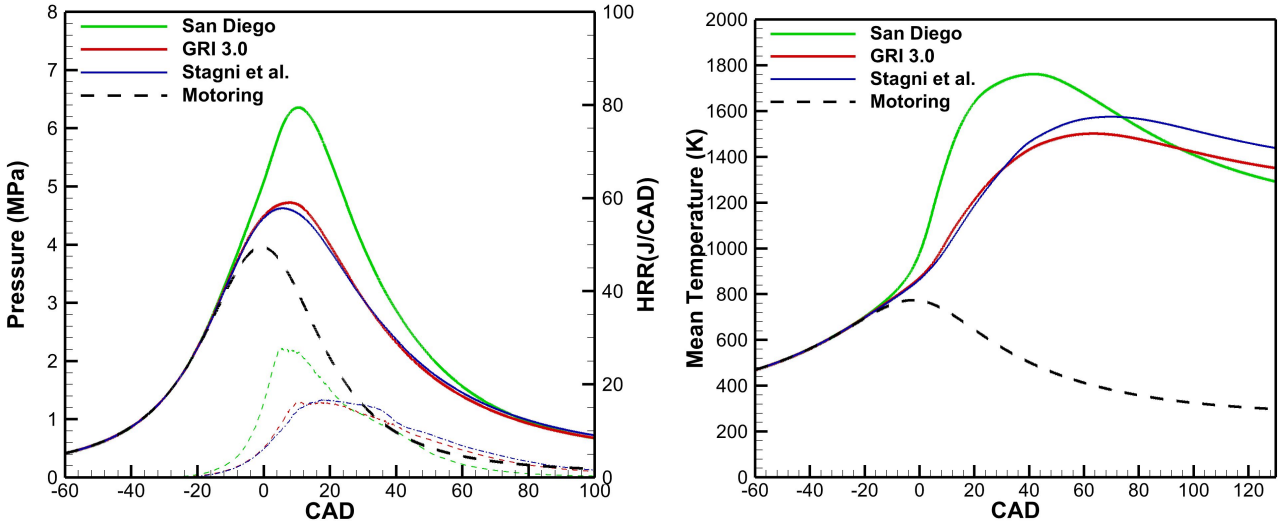

Figure 3: In cylinder pressure, HRR, and mean temperature for ammonia fueled SI engine

As mentioned earlier, the flame speed of pure ammonia is considerably low, resulting in a significantly longer ignition delay compared to conventional fuels. The ignition timing was set at -40 CAD, and the CA10 (crank angle at 10% heat release) occurs near the top dead center around 6 CAD, indicating a substantial delay in ignition and heat release rate. These findings are presented in Table 1. Furthermore, the combustion duration for a spark-ignited engine fueled with pure ammonia is considerably higher at 68.9 CAD, while for a diesel engine fueled with ammonia, it was measured at 24 CAD with AES 84% in our previous paper [7]. Furthermore, the longer duration of combustion and the main combustion phase during the expansion stroke lead to an increase in-cylinder temperature, thereby resulting in a higher exhaust gas temperature.

Table 1: Combustion indicators: CA10, CA50, CA90 and combustion duration

	CA10	**CA50**	**CA90**	**CA90-CA10**
San Diego	0.01	16.51	47.81	47.79
GRI 3.0	4.91	28.81	71.93	67.02
Stagni et al.	6.11	31.32	75.10	68.98

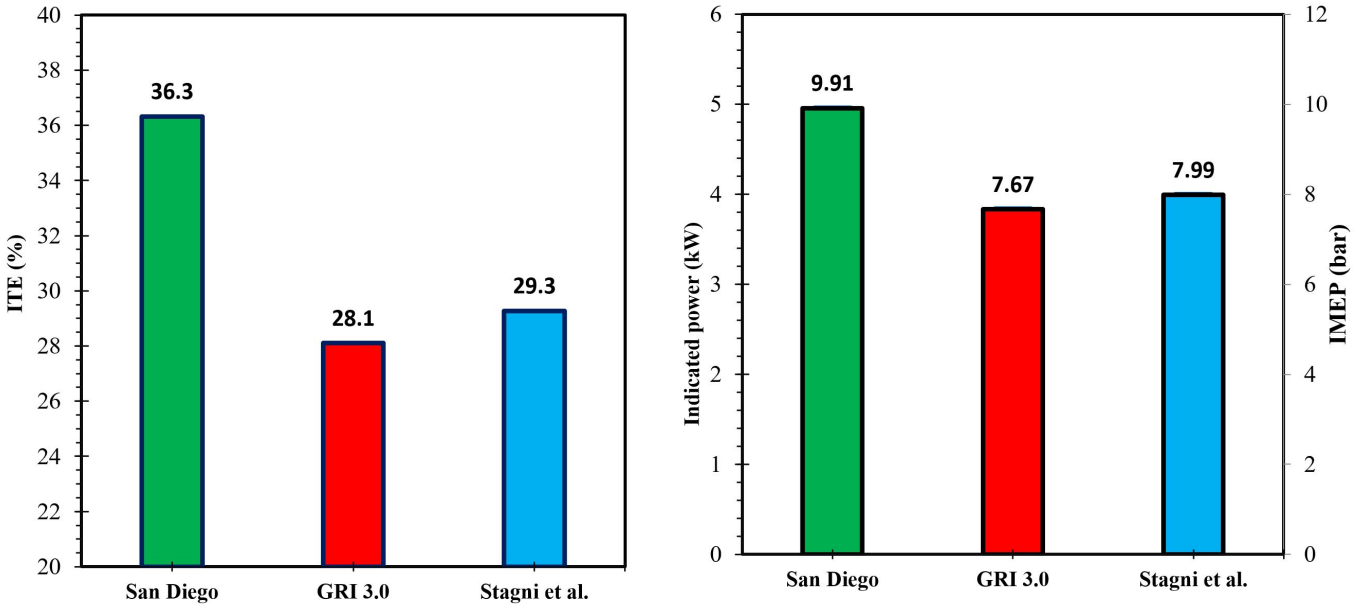

Figure 4: Indicated thermal efficiency, indicated power, and IMEP for pure ammonia fueled SI engine

The performance parameters of a SI engine fueled with pure ammonia are depicted in Figure 4. For the Stagni reaction mechanism, the IMEP is 7.99 bar at a stoichiometric ratio $\phi = 1$ and an inlet pressure $P_{in} = 1$ bar, corresponding to an indicated power of 4 kWh. Figure 4 also illustrates the indicated thermal efficiency for three different reaction mechanisms. The engine indicated efficiency is approximately 29.3%, which is relatively low mainly due to the high exhaust gas temperature and the significant amount of unburned ammonia.

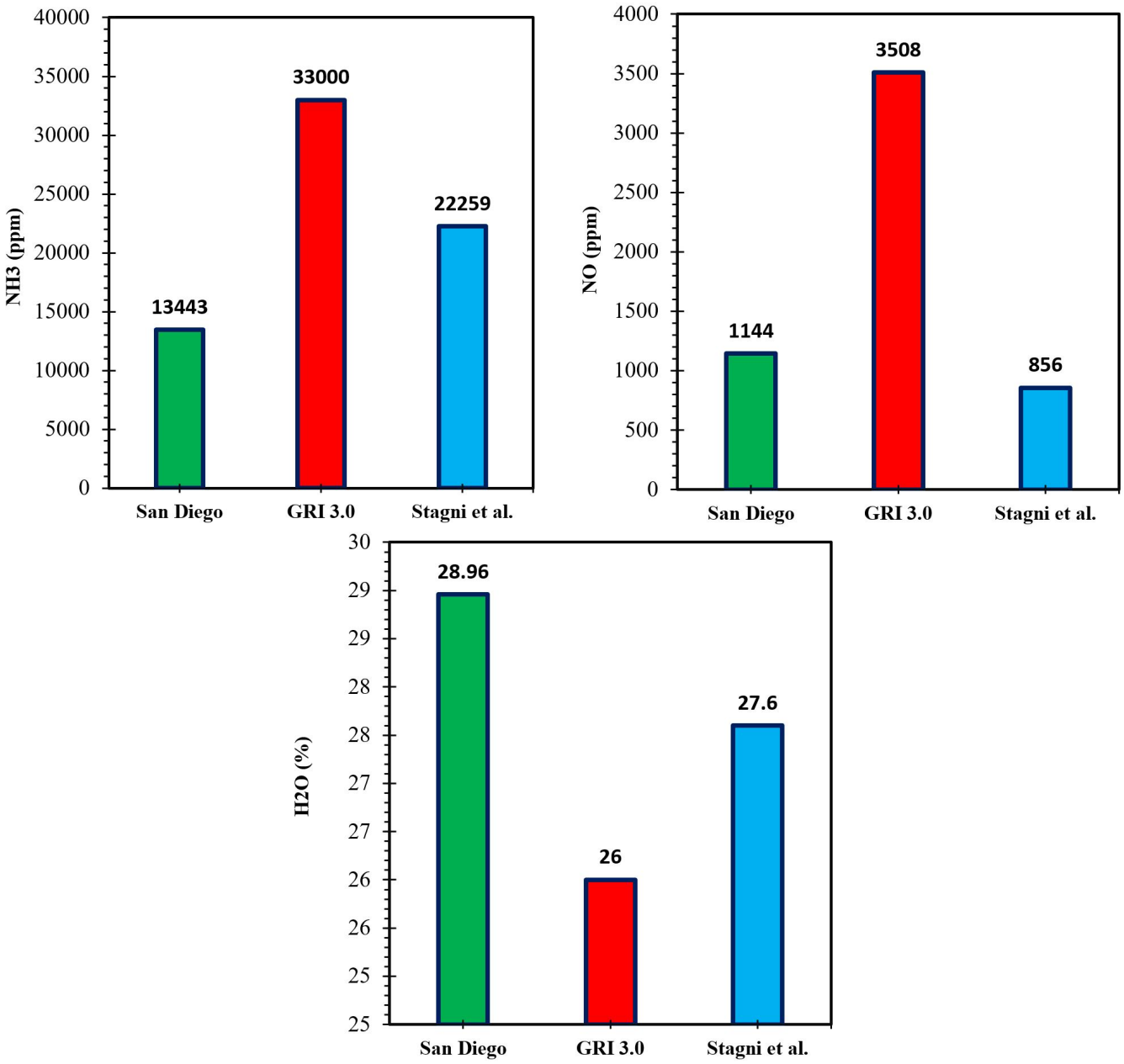

Figure 5: Ammonia, NO, and H_2O concentration in wet exhaust for pure ammonia engine operation

The exhaust emissions resulting from the combustion of pure ammonia in an SI engine are presented in Figure 5. The graph illustrates the concentrations of NH_3, NO, and H_2O in the exhaust. With the use of pure ammonia, there are no emissions of carbon-based compounds. However, a substantial amount of ammonia is emitted, measuring approximately 22,259 ppm, equivalent to 2.23% unburned ammonia. It should be noted that similar ranges of ammonia emissions have been observed in experimental data.

For the Stagni reaction mechanism, the emission of NO is approximately 856 ppm. However, the GRI 3.0 model significantly overpredicts NO emissions. Additionally, the concentration of H_2O in

the exhaust is approximately 27.6% during pure ammonia combustion. Further analysis and insights into the observed emissions will be provided in subsequent sections.

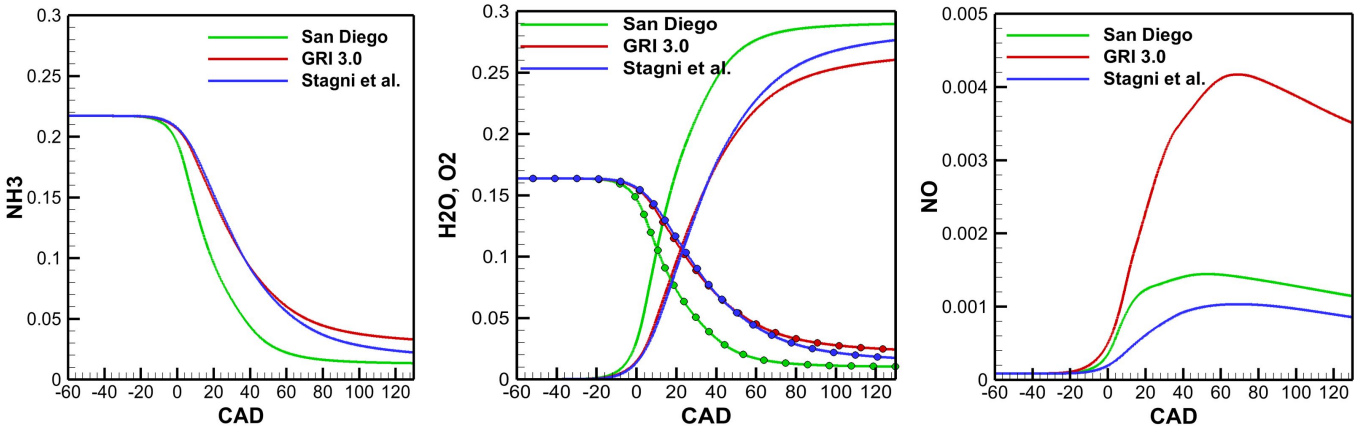

Figure 6: In cylinder mole fraction for Ammonia, NO, O_2 and H_2O in pure ammonia engine operation

Furthermore, Figure 6 provides a detailed representation of the mole fractions of NH_3, NO, and H_2O within the cylinder over the CAD. Despite the ignition timing at -40 CAD, the mole fractions of ammonia and oxygen, both start to decline as the crank angle approaches the TDC. Therefore, H_2O concentration increases after TDC, indicating evolving combustion processes. In addition, the presence of O_2 at the end of combustion indicates incomplete combustion for lambda 1. It should be noted that the GRI 3.0 reaction mechanism shows a higher mole fraction of NO compared to the other two mechanisms throughout the combustion cycle. This discrepancy emphasizes the importance of reaction mechanisms in influencing species concentrations within the combustion chamber, and further analysis is needed to validate these observed trends.

Table 2: Specific emission for pure ammonia fueled SI engine

	NH_3 (g/kWh)	NO (g/kWh)	H_2O (g/kWh)
San Diego	34.65	5.12	790.1
GRI 3.0	109.62	20.5	915
Stagni et al.	71.0	4.81	934.7

As a result, specific emissions for a pure ammonia-fueled SI engine have been calculated and are presented in Table 2. The emissions for NH_3, NO, and H_2O are quantified at 71.0, 4.81, and 934.7 g/kWh, respectively. The NO emission is comparatively low, however, unburned ammonia is significantly high. To assess the combustion efficiency of pure ammonia air combustion, the following equation was used:

$$\eta_c = \frac{m_{NH_3,in} - m_{NH_3,unburned}}{m_{NH_3,in}} \times 100\%$$

The combustion efficiency of ammonia air combustion in an SI engine is 89.2% when unburned ammonia at the exhaust is 71.0 g/kWh.

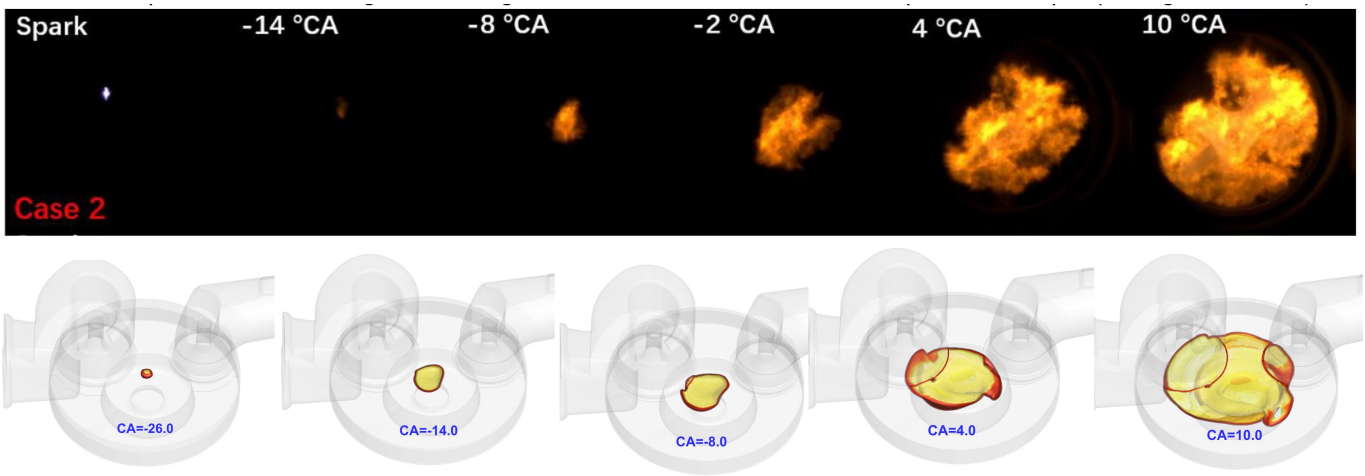

Figure 7: comparison of flame propagation between CFD simulations and experimental data obtained from Zhang et al. [8].

The comparison of flame propagation between CFD simulations and experimental data from Zhang et al. [8], is depicted in Figure 7. The experimental photographs selected for analysis cover the stages from spark time to combustion, captured through optical diagnostics. A qualitative assessment is conducted on the flame images, comparing them to the results obtained from the CFD simulations. Because of the low flame speed of ammonia, flame propagation takes a longer time. Consequently, from the ignition timing at -40 CAD to TDC (0 CAD), the ammonia flame was reached only to the piston bowl. In particular, the ammonia flame does not reach the cylinder walls during the expansion stroke., resulting in a significant amount of unburned ammonia, as can be seen in Figure 8. This observation underscores the unique characteristics of ammonia combustion and provides insight for both the experimental and simulation perspectives.

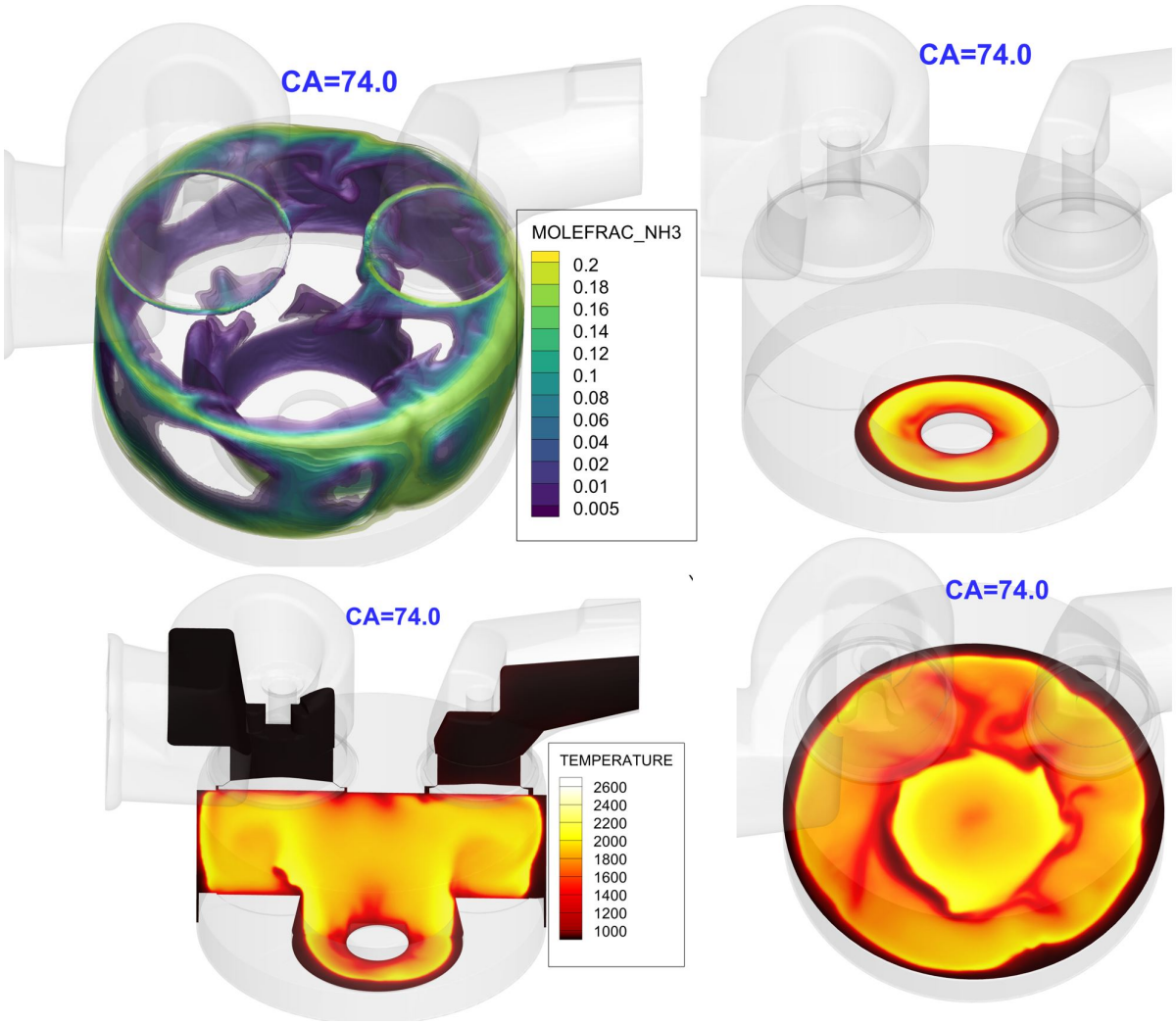

Figure 8: Iso-counter of ammonia mole fraction and in cylinder temperature distribution at CA90

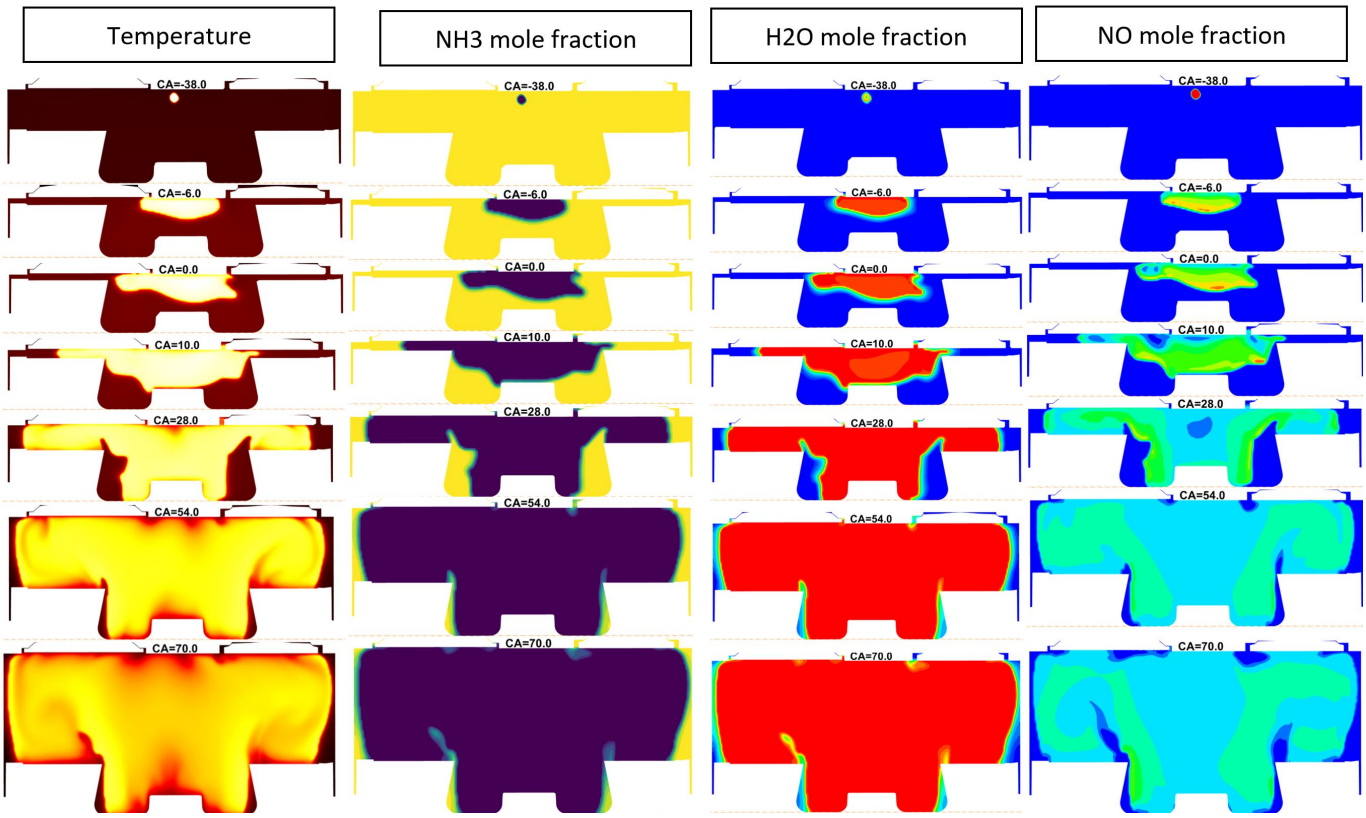

Figure 9: In-cylinder temperature, ammonia mole fraction, H_2O, and NO distribution for different CAD.

Finally, Figure 9 shows the cross-sectional contour of temperature, NH_3, H_2O, and NO at different CADs from spark to CA90 at 74 CAD. The figure highlights the absence of successful propagation of the flame around the walls and crevices of the cylinder, resulting in a notable amount of unburned ammonia.

3.2 Effect of different intake temperatures

The impact of intake temperature on the engine performance of a spark-ignited engine fueled with pure ammonia is significant. As a result of the low flame speed of ammonia, increasing the intake temperature can greatly improve the combustion process [9]. This CFD study aims to examine the effects of varying intake temperatures on the indicated thermal efficiency, emissions, and combustion characteristics of the spark-ignited engine. The ammonia-air stoichiometric mixture is heated to 350 and 400 K and compared to the base case when intake temperature at 300 K.

Figure 10 illustrates the impact of intake temperature on in-cylinder pressure, HRR, and average cylinder temperature. As the intake temperature increases, the peak pressure and HRR also increase, resulting in a more concentrated combustion phasing. The higher HRR peak indicates that higher intake temperatures enhance mixture reactivity and combustion intensity. Furthermore, elevated intake temperatures lead to faster propagation of the flame front, reaching the cylinder wall region earlier. Furthermore, increasing the intake temperature significantly raises the average temperature in the cylinder, reaching up to 1700 K.

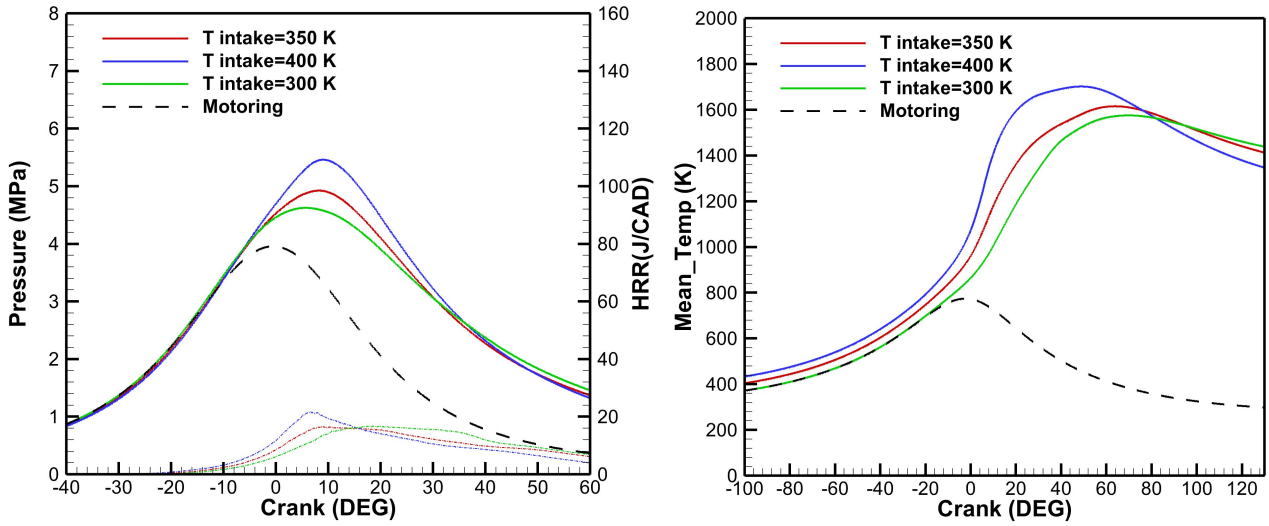

Figure 10: Effect of intake temperature on in-cylinder pressure and temperature for T=300, 350, and 400 K

Figure 11 illustrates the engine performance parameters, including IMEP, the indicated power, and ITE, at different intake temperatures. It is observed that there is a marginal decrease of approximately 3.87% in both IMEP and the indicated power with increasing intake temperature. However, increasing the intake temperature from 300 to 400 K has a significant impact on ITE, resulting in a 5 percentage point improvement. This improvement can be attributed to improved combustion and reduced ammonia emissions.

The variations in NO and NH_3 emissions corresponding to different intake temperatures are presented in Figure 12. It can be seen that as the intake temperature increases, the NO emission increases from 856 ppm at T_{in} = 300 K to 1154 ppm at T_{in} = 400 K due to the higher combustion

temperature. However, increasing the intake temperature by 100 K leads to a significant reduction in ammonia emission from 22,259 to 13,140 ppm. Also, the combustion efficiency improved from 89.2 to 93.6% and ammonia emission was reduced similarly from 71.0 to 36.8 g/kWh for $T_{in} = 400$ K.

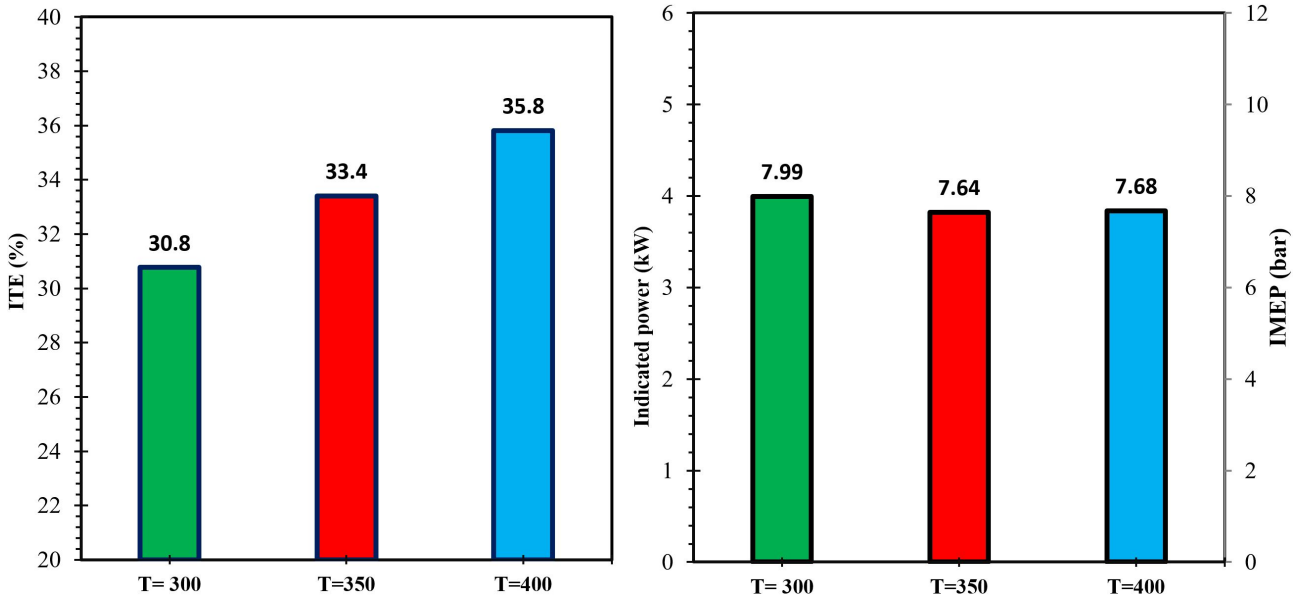

Figure 11: Effect of intake temperature on indicated power, efficiency, IMEP for T=300, 350, and 400 K.

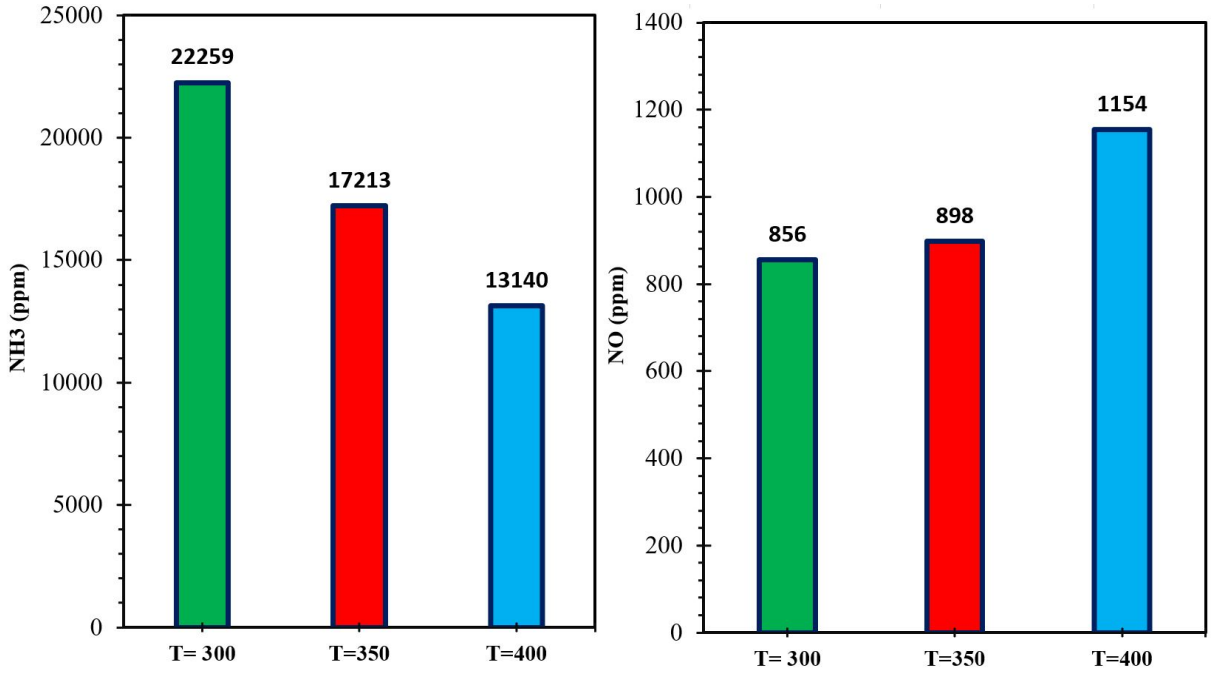

Figure 12: Effect of intake temperature of $T_{in} = 300$, 350, and 400 K on ammonia and NO emissions.

4 Experimental result of pure ammonia fueled SI engine

The CI engine has been modified to allow pure ammonia combustion. This involved installing a spark plug in the engine head and introducing gaseous ammonia into the intake manifold. The performance of the pure ammonia-fueled SI engine was tested at different lambda values $\lambda = 1, 1.2, 1.3$ and with ignition timing ranging (α_{ign}) from 15 to 50 before TDC.

Figure 13 depicts the experimental IMEP and COV_{IMEP} for an ammonia-fueled SI engine. It can be seen that the engine can be run with different ignition timing and lambda. However, increasing lambda leads to higher COV_{IMEP} values, indicating unstable engine operation. Similarly, the close ignition timing to the TDC also increased COV_{IMEP} since the ammonia flame speed in low ammonia needs more time for combustion. Therefore, increasing ignition timing improves IMEP and indicated efficiency, as can be seen in figure 14. The maximum IMEP was obtained at 9 bar for the stoichiometric mixture.

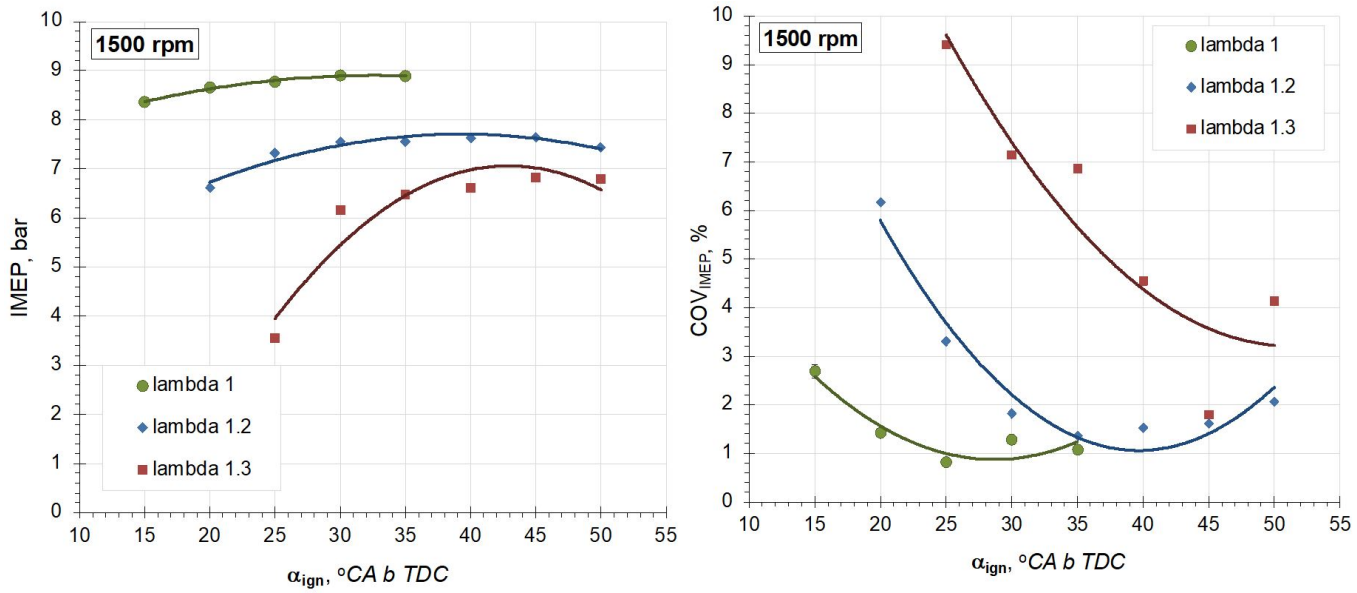

Figure 13: IMEP and COV of IMEP of pure ammonia fueled engine for different lambda and ignition timing

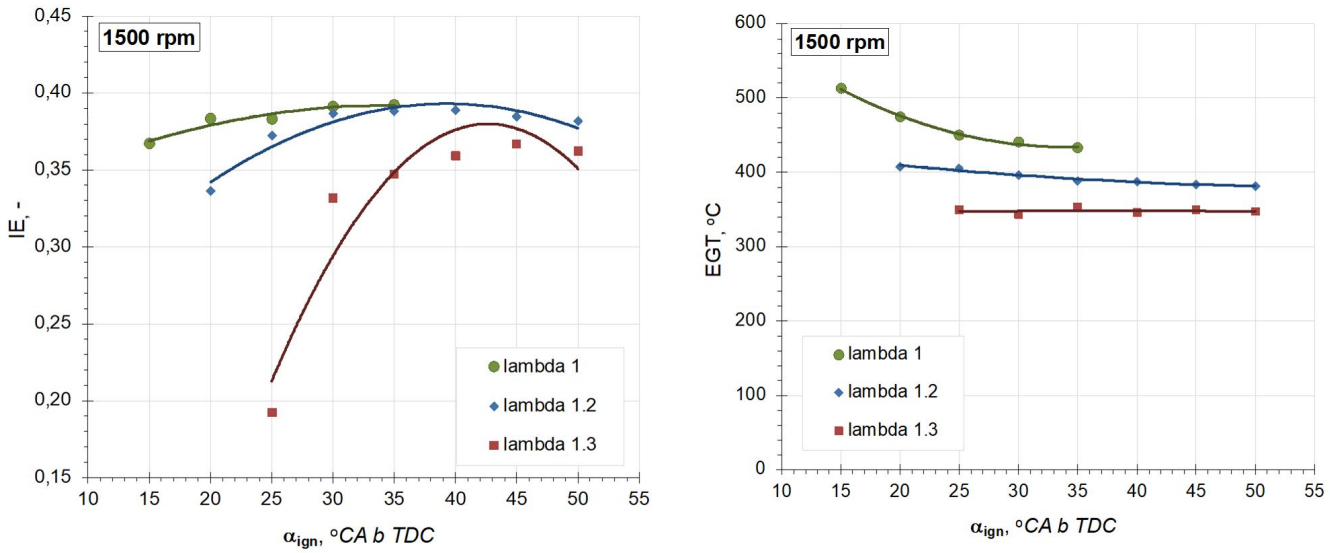

Figure 14: Indicated efficiency and exhaust gas temperature of pure ammonia fueled engine for different lambda and ignition timing

The highest efficiency of around 35% is achieved at lambda values of 1 and 1.2, with an ignition timing of 35 bTCD.

Figure 5 shows the exhaust emissions resulting from the combustion of pure ammonia in an SI engine, including the concentrations of NH_3, NO, NO_2 and N_2O in the exhaust measured with FTIR. When pure ammonia is used, there are no emissions of carbon-based compounds. However, a significant amount of unburned ammonia is emitted, measuring approximately in range 1.8% to 2.5% in wet exhaust. Also, by increasing lambda, the ammonia emission increased. NO, NO_2 and N_2O emission for various ignition timings are shown in figure 15. It can be seen that early ignition time at 50 CA increases NO and NO_2 emissions. However, N_2O has opposite trend and lowest N_2O emission around 36 ppm were achieved at $\lambda = 1$ and spark time of 30 CA bTDC.

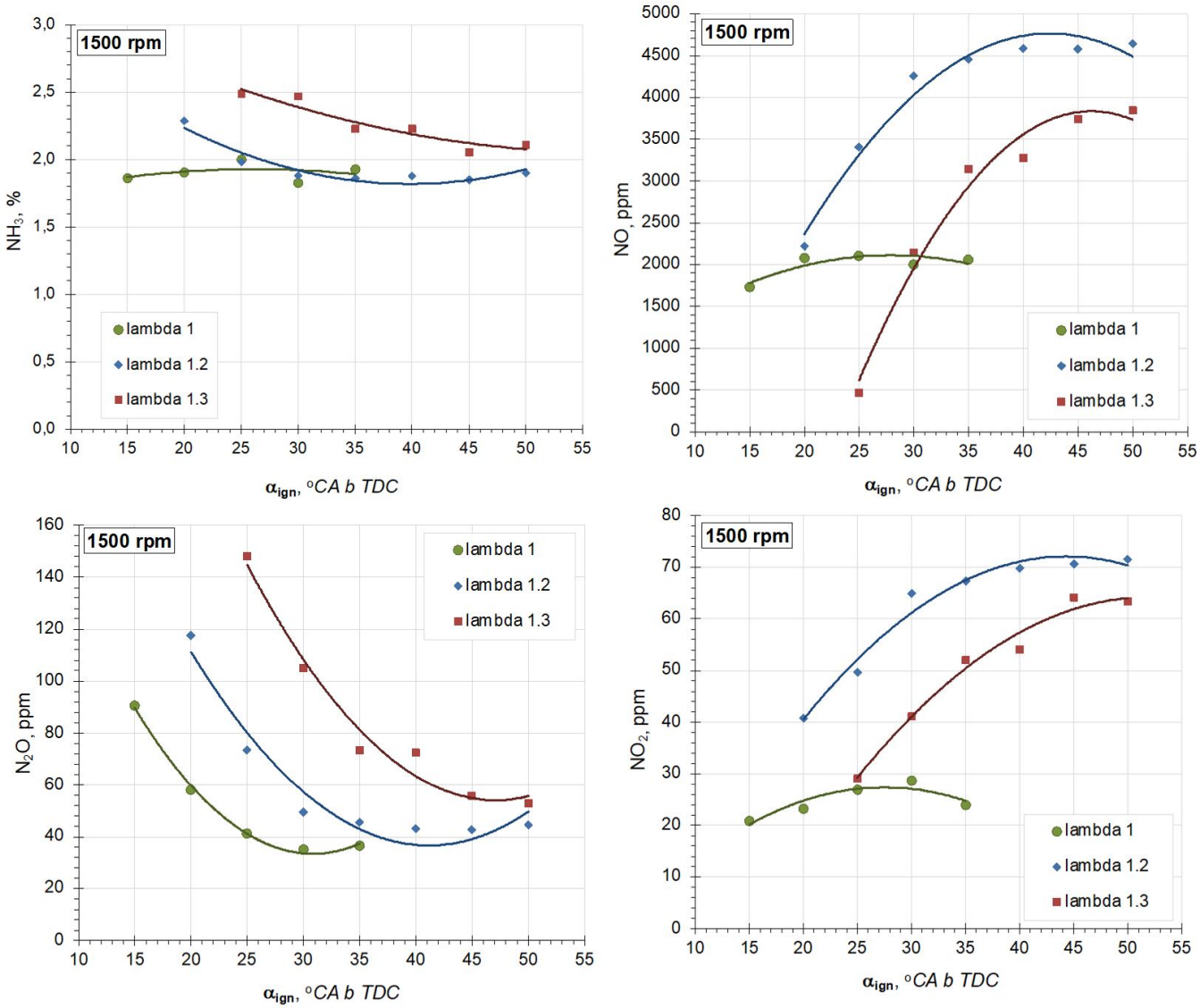

Figure 15: Emission of pure ammonia fueled engine for different lambda and ignition timing

Based on the results, pure ammonia-fueled SI engines can be operated successfully if the spark timing is significantly advanced. However, it is important to note that ammonia flames have extremely low flame speed, which results in longer ignition delays and combustion durations, as well as a lower peak heat release rate. Additionally, the unburned ammonia is significantly higher in pure ammonia-fueled SI engines.

5 Environmental and economical sustainability of ammonia driven SI engine

5.1 Environmental analysis

The sustainability of ammonia-powered SI engines in agriculture to consider in 4SCE application for powering and heating purposes hinges on various elements like agricultural types, operational scale, and regional climate. For example, Swedish dairy farms use 930 to 1540 kWh per cow per year, leading to 0.125-0.203 kWh per liter of milk, with 65%-75% of energy dedicated to milking and feeding. In piglet production, the energy need is 689 kWh per sow annually or 28.7 kWh per 25 kg piglet, assuming 24 piglets per sow per year. Energy demands in egg production differ with housing type: 3.1 kWh/hen in furnished cages versus 5.0 kWh/hen in free-range systems, primarily for lighting and ventilation [10].

In this report, a small power ammonia SI engine is analyzed operating at 1500 rpm (3 kWel of power for a single cylinder). The environmental and economic analyses aim to compare this engine with a typical diesel generator, focusing on general rather than case-specific performance. These engines are designed to provide electrical energy and heat during peak loads or grid issues, applicable to any farm type. The environmental analysis examines emissions from both engine operation and fuel production pathways. It is assumed that the manufacturing and utilization phases of the SI engine body are similar to those of a diesel generator of the same size, thereby not affecting the overall conclusions.

The technical analysis of the SI engine was conducted by reviewing the available literature, primarily from [11]. This study focused on a 4-cylinder, 4-stroke Gasoline Direct Injection-SI EP6 PSA modified to operate on a single cylinder. A hydrogen-ammonia fuel mixture was utilized to enhance combustion. The technical data employed in this analysis are presented in Table 3. These values were derived mainly from [11], except for the indicated efficiency, which was assumed based on [12] for a comparable engine operating at 1500 rpm. Additionally, the mechanical and generator efficiencies were estimated based on typical efficiencies for such devices.

The technical assessment of the engine was conducted using the following methodology:

1. Calculated the indicated, brake, and electrical power based on the technical data and associated efficiencies.
2. Estimated ammonia and hydrogen fuel mass flow rates from the fuel input.
3. Determined the exhaust mass flow rate and its composition from stoichiometric calculations, adjusting for the amount of ammonia present in the exhaust (exhaust composition for enthalpy calculation included ammonia, oxygen, nitrogen, and water vapor).
4. Estimated the calculated electrical power of the engine to be 2.82 kW.
5. Estimated the thermal power of the engine to be 3.27 kW, assuming heat exchanger cooling of the exhaust to 120 °C.

Table 3: Technical specification of SI engine based on [11].

Parameter	Value	Unit
Revolutions per minute, RPM	1500	-
Displacement volume, V_d	399.5	cm3
Intake pressure, P_{in}	1	bar
Equivalence ratio, Φ	1	-
Indicated mean effective pressure, IMEP	7	bar
Exhaust temperature	500	°C
H2, vol. fuel share	10	%
NH3, vol. fuel share	90	%
NOx, exhaust	2000	ppm
N2O, exhaust	50.5	ppm
NH3, exhaust	0.77	%
Indicated efficiency, η_{ind}	32	%
Mechanical efficiency, η_m	85	%
Generator efficiency, η_g	95	%

Based on the calculations, the input-output analysis was determined in terms of the fuel consumption as well as the emissions. This is shown in Table 4 for 1000h operation time. The data for the diesel generator was taken from the SUT laboratory tests performed on the Lifan C186F engine presented in the paper [13]. Since the analysis regards the 4SCE application, a linear scaling is assumed, i.e. all cylinders operate under the same conditions.

Table 4: Input-output analysis of ammonia SI engine for 1000h operation time (single cylinder).

Electrical energy	2823	kWh
Thermal energy	3265	kWh
Ammonia fuel consumption	2105.56	kg
Hydrogen fuel consumption	27.52	kg
NH3	120.67	kg
O2	170.36	kg
N2	12078.45	kg
H2O	8605.48	kg
NOX	55.31	kg
N2O	2.05	kg

The technical performance between the two options for 1000h at 4 cylinder operation is compared in the Table 5. Ammonia SI generator is characterized by higher exhaust temperature as well as the mass flow rate which results in considerable increase in the heat production. This could be desired, depending on the specific application.

Table 5: Technical performance comparison of the two generators.

	Electrical energy, kWh	Thermal energy, kWh
Ammonia SI generator	11290.87	13061.07
Diesel generator	11036.92	6770.472

Based on the technical analysis of the two engines, an environmental analysis was conducted using the LCA for Experts (GaBi) software, employing the ReCiPe 2016 v1.1 method for Life Cycle Impact Assessment. The comparison is based on 1000 hours of operation with a 4-cylinder setup. The fuel production pathways are in accordance with the D 5.6 report, including:

1. Grey ammonia - produced through steam methane reforming.
2. Blue ammonia - produced through steam methane reforming with carbon capture and storage.
3. Green ammonia - produced through water electrolysis, powered by electrical energy from photovoltaic or wind sources.
4. Pink hydrogen - produced through water electrolysis, powered by electrical energy from a nuclear source.

The results concerning climate change, human health, and ecosystem quality of the analyzed cases are presented respectively in Figures 16, 17, and 18. When ammonia is produced from renewable or nuclear sources, a 50-60% reduction in greenhouse gas emissions is achieved. This could be further optimized by reducing N2O emissions from the engine. From the endpoint categories perspective, ammonia and NOx present in the exhaust contribute more to environmental damage compared to PM and hydrocarbons from diesel. This underscores the need for effective mitigation strategies for both NOx and NH3 emissions. According to the findings in the D 5.6 report, while the SCR unit can substantially reduce NOx, a high NH3 concentration remains in the exhaust. The SCR unit was not included in [11] and thus was not considered in this analysis.

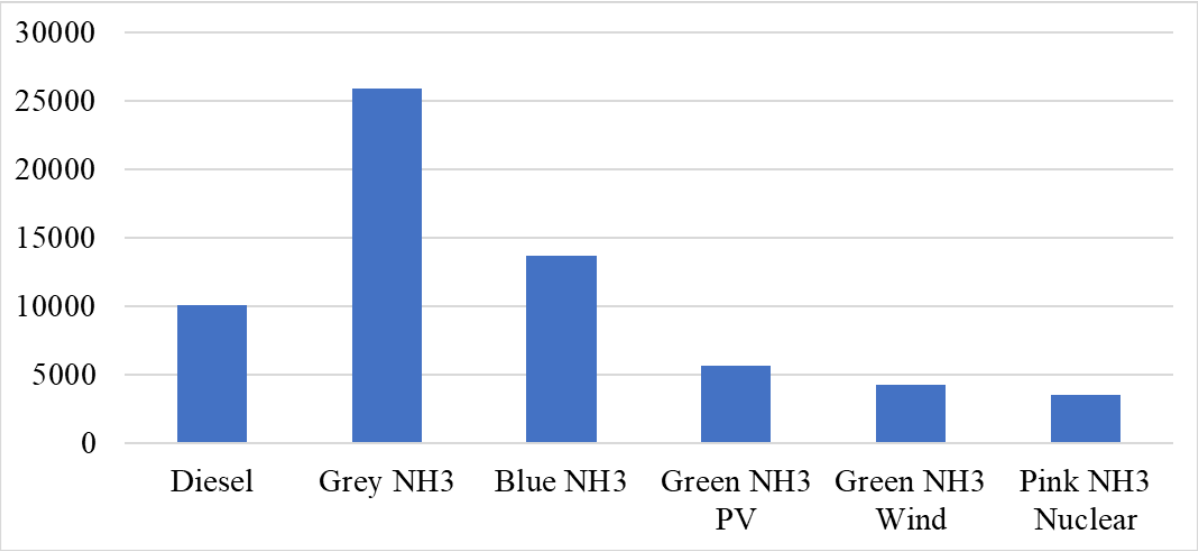

Figure 16: Climate change results of 4SCE for 1000 hours.

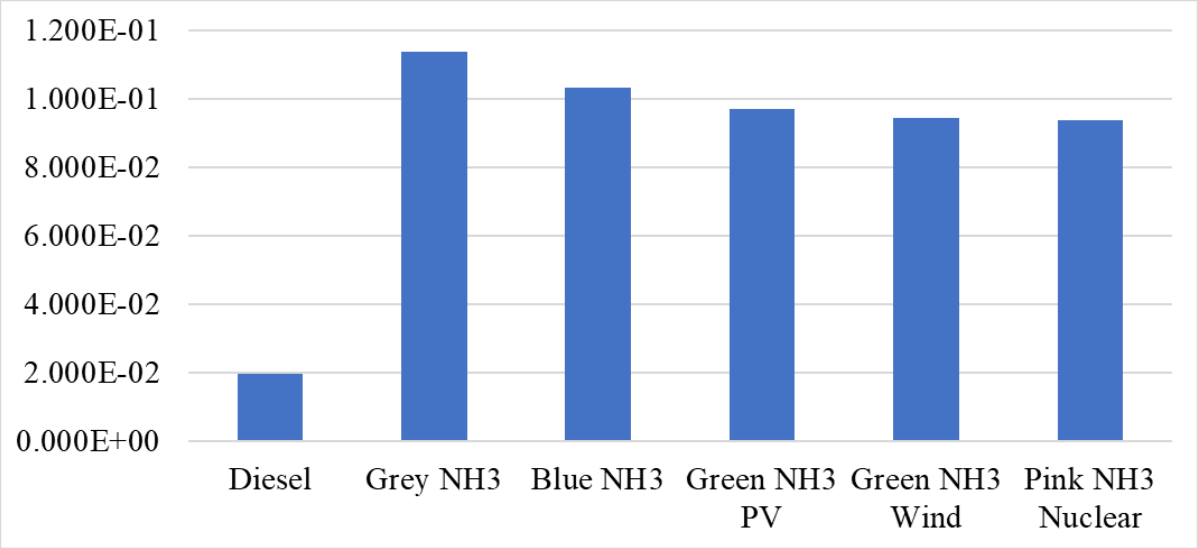

Figure 17: Human health results of 4SCE for 1000 hours.

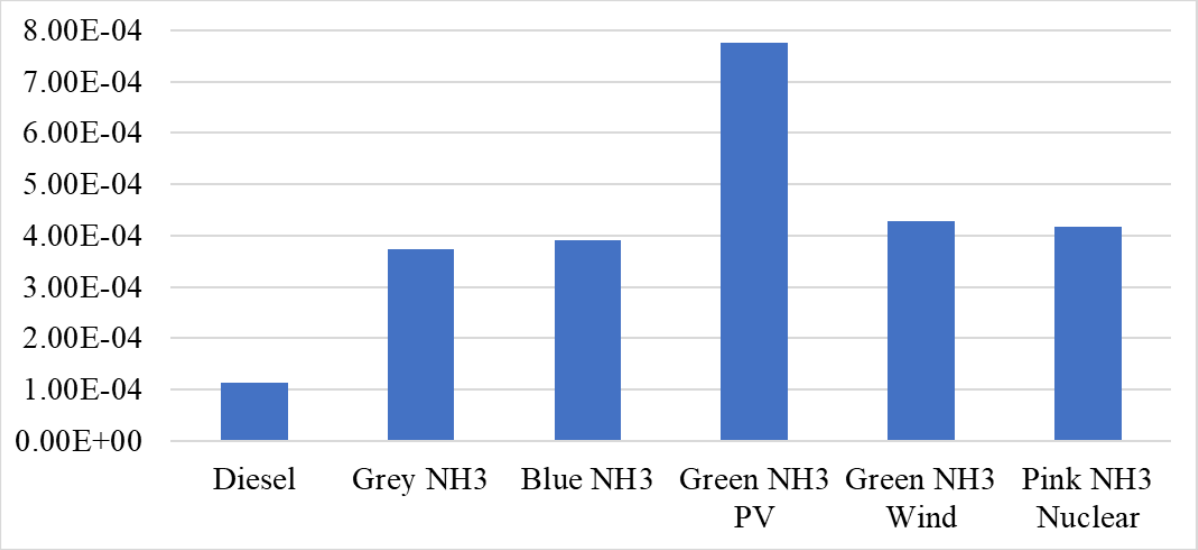

Figure 18: Ecosystem quality results of 4SCE for 1000 hours.

5.2 Economic analysis

The economic comparison between the two engine types takes into account both the capital cost of acquiring the engine and the ongoing costs associated with fuel consumption. Given that the engines under consideration are of a small power rating, certain cost factors, such as emissions-related expenses, are not applicable. Specifically, in Poland, the obligation to incur emissions costs is contingent upon the energy output provided by the fuel at nominal load. This is governed by the Regulation of the Minister of the Environment dated July 2, 2010, which stipulates that emissions from installations do not require a permit unless the installation's output exceeds 10 MW. Consequently, for diesel installations with an output lower than this threshold, emissions costs are not incurred.

The capital expenditure for a standard 12 kWel diesel generator in a Combined Heat and Power (CHP) unit is estimated at approximately 4000 USD, based on current market research. According to the economic assessment detailed in document D 5.7, it has been observed that the capital cost for an ammonia-fueled engine with direct injection (DI) is roughly double that of a diesel engine in similar applications. While this cost multiplication factor is primarily associated with the modifications required for ammonia fuel management. It is generally understood that, for equivalent power outputs, SI engines are less expensive than diesel engines, with a conservative estimate indicating that an SI engine may cost approximately 25% less than a comparable diesel engine. This price reduction is reflective of the different manufacturing processes and material requirements inherent to SI engines. Taking these factors into account the estimated cost for an ammonia SI engine is projected at 6000 USD. This estimation serves as a tentative figure, reflecting the combined effects of the diesel-to-ammonia conversion premium and the intrinsic cost differences between diesel and SI engines. It must be emphasized, however, that these figures are derived from broad market trends and documented conversion costs and may not encapsulate all the nuanced economic factors. The estimates would benefit from further refinement through detailed consultations with industry experts.

The operational costs are in line with the assumptions presented in the D 5.7 for the prices of fuels. Aggregating the capital, operational and End of Life (EoL) costs, the Total Cost of Ownership (TCO) can be obtained. The assumptions for the economic analysis can be summarized as follows:

1. The engine is operated for the period of 10 years at 1000h annually.
2. Maintenance costs are fixed at an annual rate of 5% of the engine price.
3. Diesel pricing is averaged from the spot prices at New York Harbor, U.S. Gulf Coast, and Los Angeles, as reported by the U.S. Energy Information Administration for 2022. A 15% increment over the spot price is applied to account for the wholesale purchase, amounting to a wholesale price of 4.13 USD/gallon.
4. The wholesale price for natural gas is derived from the 2022 Henry Hub price, as per the U.S. Energy Information Administration, equating to 7.42 USD/MMBtu.
5. Industrial electricity rates are taken from 2022 data provided by the U.S. Energy Information Administration, resulting in a cost of 83.2 USD/MWh.
6. End of Life (EoL) costs are projected to be 20% of the vehicle's capital cost, an estimation aligned with industry literature [**?**].

Total Cost of Ownership comparison for selected ammonia sources is presented in the Figure 19. It is shown that for applications, the price of fuel determines the profitability of an investment. For SI ammonia generator, higher fuel consumption on a mass basis along with higher capital cost, result in total cost increment. This could be reduced if the owner benefited from incentives from using carbon free fuel, however these are typically available for industry that use big-power applications. The most costly solution is the electrolysis based green ammonia.

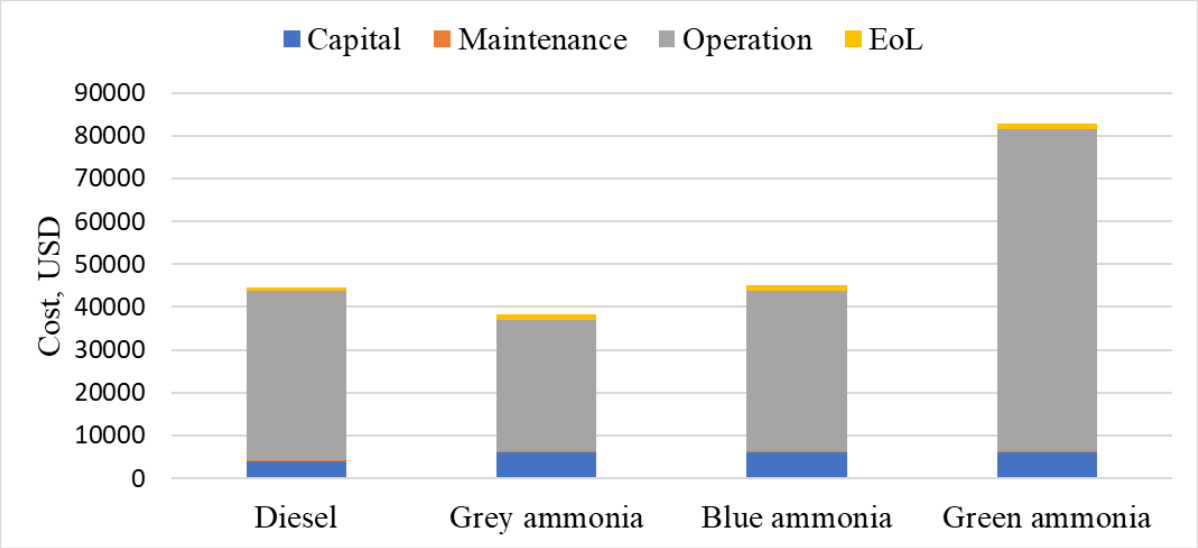

Figure 19: Total Cost of Ownership results.

5.3 Summary

The SI ammonia engine offers significant decarbonization potential. Utilizing ammonia derived from renewable or nuclear sources can lead to a 50-60% reduction in greenhouse gas emissions, predominantly during the fuel production phase. Additionally, minimizing N2O emissions during the engine's operation could further enhance environmental benefits. However, in terms of human health and ecosystem quality, ammonia and NOx emissions from the exhaust are more detrimental compared to particulate matter and hydrocarbons from conventional diesel engines. Hence, developing effective mitigation strategies for NOx and NH3 emissions is crucial for future research, especially since current Selective Catalytic Reduction (SCR) units, while effective at reducing NOx, allow for high ammonia levels in the exhaust.

From an economic perspective, the analysis indicates that electrolysis-based ammonia production is currently the most costly, primarily due to the high assumed electricity price of 83.2 USD/MWh. For ammonia-fueled SI engines to be cost-competitive with diesel, electricity costs would need to fall to around 40 USD/MWh or lower. While achievable, such prices are currently on the lower end of the spectrum. However, government incentives for using carbon-free fuels could substantially enhance the economic feasibility of this technology.

References

[1] Charles Lhuillier, Pierre Brequigny, Francesco Contino, and Christine Mounaïm-Rousselle. Experimental study on ammonia/hydrogen/air combustion in spark ignition engine conditions. *Fuel*, 269:117448, 2020.

[2] Jinguang Li, Ren Zhang, Jiaying Pan, Haiqiao Wei, Gequn Shu, and Lin Chen. Ammonia and hydrogen blending effects on combustion stabilities in optical si engines. *Energy Conversion and Management*, 280:116827, 2023.

[3] Ebrahim Nadimi, Grzegorz Przybyła, Terese Løvås, Grzegorz Peczkis, and Wojciech Adamczyk. Experimental and numerical study on direct injection of liquid ammonia and its injection timing in an ammonia-biodiesel dual injection engine. *Energy*, 284:129301, 2023.

[4] Alessandro Stagni, Carlo Cavallotti, Suphaporn Arunthanayothin, Yu Song, Olivier Herbinet, Frédérique Battin-Leclerc, and Tiziano Faravelli. An experimental, theoretical and kinetic-modeling study of the gas-phase oxidation of ammonia. *Reaction Chemistry & Engineering*, 5(4):696–711, 2020.

[5] Gregory P Smith. Gri-mech 3.0. *http://www. me. berkley. edu/gri_mech/*, 1999.

[6] FA Williams. Chemical-kinetic mechanisms for combustion applications. san diego mechanism web page, mechanical and aerospace engineering (combustion research), at san diego.(2018), 2014.

[7] Ebrahim Nadimi, Grzegorz Przybyła, Michał T Lewandowski, and Wojciech Adamczyk. Effects of ammonia on combustion, emissions, and performance of the ammonia/diesel dual-fuel compression ignition engine. *Journal of the Energy Institute*, 107:101158, 2023.

[8] Ren Zhang, Lin Chen, Haiqiao Wei, Jinguang Li, Rui Chen, and Jiaying Pan. Understanding the difference in combustion and flame propagation characteristics between ammonia and methane using an optical si engine. *Fuel*, 324:124794, 2022.

[9] Xiaozhong Hu, Jiaying Pan, Ren Zhang, Jinguang Li, Wei Li, and Haiqiao Wei. Effects of intake parameters and compression ratio on ammonia combustion and emissions in si engines. *Fuel*, 354:129382, 2023.

[10] Torsten Hörndahl. Energy use in farm buildings. Report, Faculty of Landscape Planning, Horticulture and Agricultural Sciences, Swedish University of Agricultural Sciences, 2008.

[11] Christine Mounaïm-Rousselle, Pierre Bréquigny, Clément Dumand, and Sébastien Houillé. Operating limits for ammonia fuel spark-ignition engine. *Energies*, 14(14), 2021.

[12] Charles Lhuillier, Pierre Brequigny, Francesco Contino, and Christine Mounaïm-Rousselle. Performance and emissions of an ammonia-fueled si engine with hydrogen enrichment. 09 2019.

[13] Mateusz Proniewicz, Karolina Petela, Andrzej Szlek, Grzegorz Przybyła, Ebrahim Nadimi, Łukasz Ziółkowski, Terese Løvås, Wojciech Adamczyk, et al. Energy and exergy assessments of a diesel-, biodiesel-, and ammonia-fueled compression ignition engine. *International Journal of Energy Research*, 2023.